FEATURE AIDED SWITCHING MODEL SET APPROACH FOR MANEUVERING TARGET TRACKING

J.-P. Fan, Y.-L. Zhu, S.-J. Fan*, H.-Q. Fan, and Q. Fu

ATR Key Laboratory, National University of Defense Technology, Changsha, Hunan 410073, P. R. China

Abstract—Feature aided maneuver detector is popular for its low detection delay and high detection probability in decision-based single-model maneuvering target tracking (MTT) algorithms. We propose a switching model-set approach based on the feature aided maneuver detector for MTT. The filtering error dynamics in terms of detection delay are presented and a upper bound for detection delay with given standard Kalman filtering errors is accessed. Subsequently, a feature aided maneuver detector is introduced to enhance detection performance, and the filtering algorithm is proposed, including detailed filtering steps and computational formulae. Simulation results show that the proposed algorithm outperforms the popular autonomous multiple model (AMM) and interacting MM (IMM) algorithms.

1. INTRODUCTION

The maneuvering target tracking (MTT) problem has been a hot topic for many years in the field of state estimation [1, 2]. Since target acceleration cannot be measured directly by existing sensors, maneuvering target tracking turns out to be a hybrid estimation problem [3, 4]. Current MTT algorithms mostly deal with the target motion uncertainty, including decision-based single-model method and multiple-model method [3, 5]. The multiple-model method, although excellent in quality and reliability, is computationally inefficient. In fact, in applications like guidance and navigation, the other method, the decision-based single-model one is much more appealing due to its low computational complexity. Given a timely maneuver detector, the decision-based single-model method has been shown to achieve

a tracking accuracy similar to that of multiple-model method [6], therefore is very favorable in resource-limited scenarios. The key component lies in the correct and timely maneuver detection.

At present, most maneuver detection algorithms are developed based on the innovation information, but provide large detection delay and low detection probability [4]. Optical image-based detection algorithms reduce detection delay, but increase system complexity. In addition, optical sensors are susceptible to weather conditions, therefore is only suitable for short or medium range scenarios [7]. Recently, a novel group of algorithms called feature aided target maneuver detection are proposed, and they are dependent on radar signatures. For instance, boresight error signal, echo amplitude fluctuations, and even two-dimensional range-Doppler images are utilized for maneuver detection [8–10]. The authors have proposed an effective algorithm based on the differences in high resolution Doppler profile (HRDP) [11]. These feature aided algorithms reduce detection delay, increase detection probability, and improve detection performance significantly. However, how to integrate the feature aided detector into tracking filter and evaluate its performance remains unaddressed.

As we know, the target non-maneuver behavior can be accurately portrayed with a single mode, while multi-models are needed to accurately demonstrate the large maneuver behavior (The direction and intensity are not known a prior). We propose a novel feature aided switching model set approach for MTT in this paper. Firstly, based on the feature aided maneuver detector, the target motion can be divided into two types: non-maneuver and maneuver. When the target maneuvered, the multi-model identification techniques can be used to distinguish between multiple maneuver models. It is a multi-level classification method and the state filter is a variable structure multiple mode (FA-VSMM) filter. The FA-VSMM method not only improves the accuracy of motion pattern recognition of decision-based single-model method, but also reduces the computational load of multiple-model method.

The remainder of the paper is organized as follows. Section 2 presents error dynamics in terms of detection delay, and accesses an allowed detection delay upper bound for given filtering errors. A brief introduction of our feature aided maneuver detector is given in Section 3. Section 4 presents the filtering algorithm, including state space model and detailed filtering steps. Simulation experiments are performed in Section 5. Finally, the conclusions are drawn in Section 6.

2. DETECTION DELAY AND ERROR DYNAMICS

Due to the existence of maneuver detection delay, target motion mode and the filtering model are mismatching. This will lead to greater filtering errors, even divergence. It is thus important to quantify error dynamics in terms of detection delay, and access an upper bound for detection delay with given filtering errors.

Assumed that nonmaneuvering and maneuvering motion modes can be described by two generic types of models: the constant velocity (CV) model and constant turn (CT) model with a known turn rate. The state equation is

$$\mathbf{x}_{k+1} = \mathbf{\Phi}^i \mathbf{x}_k + \mathbf{w}_k \quad (i = \text{CV, CT}) \tag{1}$$

where,

$$\mathbf{x} = \begin{bmatrix} x \\ \dot{x} \\ y \\ \dot{y} \end{bmatrix}; \quad \mathbf{\Phi}^{\text{CV}} = \begin{bmatrix} 1 & T & 0 & 0 \\ 0 & 1 & 0 & 0 \\ 0 & 0 & 1 & T \\ 0 & 0 & 0 & 1 \end{bmatrix};$$

$$\mathbf{\Phi}^{\text{CT}} = \begin{bmatrix} 1 & \frac{\sin \omega T}{\omega} & 0 & -\frac{1-\cos \omega T}{\omega} \\ 0 & \cos \omega T & 0 & -\sin \omega T \\ 0 & \frac{1-\cos \omega T}{\omega} & 1 & \frac{\sin \omega T}{\omega} \\ 0 & \sin \omega T & 0 & \cos \omega T \end{bmatrix}$$

The state vector $\mathbf{x}$ contains the coordinate (x, y) and velocity $(\dot{x}, \dot{y})$ of the target. The $\mathbf{\Phi}^{\text{CV}}$ and $\mathbf{\Phi}^{\text{CT}}$ are respective transpose metrics of CV and CA model. The process noise $\mathbf{w}$ is zero-mean Gaussian white noise, and its covariance matrix is omitted here which can be found in [12]. It is noted that $\mathbf{\Phi}^{\text{CV}} = \mathbf{\Phi}^{\text{CT}} \ (\omega = 0)$.

Assumed that target position is measurable, and the measurement equation is

$$\mathbf{z}_k = \begin{bmatrix} x_k^m \\ y_k^m \end{bmatrix} = \begin{bmatrix} 1 & 0 & 0 & 0 \\ 0 & 0 & 1 & 0 \end{bmatrix} \mathbf{x}_k + \begin{bmatrix} v_k^x \\ v_k^y \end{bmatrix} = \mathbf{H}\mathbf{x}_k + \mathbf{v}_k \tag{2}$$

where, $\mathbf{z}$ is the measurement vector, $\mathbf{v}$ the measurement noise with zero-mean Gaussian distribution, and $\mathbf{H}$ the measurement matrix.

(1) and (2) constitute a linear Gaussian hybrid system. Kalman filter is an approximately optimal estimator for the base-state. Although the filtering models are different, Kalman gains and estimation error covariance matrices have the same iteration forms.

$$\begin{cases} \mathbf{P}_{k+1|k}^i = \mathbf{\Phi}^i \mathbf{P}_{k|k}^i \left[\mathbf{\Phi}^i \right]^T + \mathbf{Q}_k^i \\ \mathbf{K}_{k+1}^i = \mathbf{P}_{k+1|k}^i \mathbf{H}^T \left(\mathbf{H} \mathbf{P}_{k+1|k}^i \mathbf{H}^T + \mathbf{R}_{k+1} \right)^{-1} \\ \mathbf{P}_{k+1|k+1}^i = \mathbf{P}_{k+1|k}^i - \mathbf{K}_{k+1}^i \left(\mathbf{H} \mathbf{P}_{k+1|k}^i \mathbf{H}^T + \mathbf{R}_{k+1} \right) \left[\mathbf{K}_{k+1}^i \right]^T \\ \qquad\qquad\qquad\qquad\qquad\qquad\qquad (i = \text{CV, CT}) \end{cases} \tag{3}$$

We omit the superscript i, and the denotations $\mathbf{K}_k^i$ and $\mathbf{P}_{k|k}^i$ are simplified as $\mathbf{K}_k$ and $\mathbf{P}_{k|k}$. The following two conditions are assumed to be true for motion mode switching and maneuver detection.

(1) Target maneuvering motion mode started at the time k_o can be correctly detected at the time k_o' as shown in Fig. 1;

(2) The maneuvering motion mode sojourn time $k_t - k_o$ is greater than detection delay.

In Fig. 1, k_o and k_t are the maneuver onset and termination times respectively. k_s is the time when the tracking filter is convergent and stable. Under the above two conditions, the mode transition of the hybrid system is observable [13]. As target maneuver onset detection is more important [1], we only consider the time interval $k_s \leq k < k_o'$, CV model is utilized for filtering, and the state estimate is

$$\hat{\mathbf{x}}_{k+1|k+1} = (\mathbf{I} - \mathbf{K}_{k+1}\mathbf{H})\,\boldsymbol{\Phi}^{\mathrm{CV}}\hat{\mathbf{x}}_{k|k} + \mathbf{K}_{k+1}\mathbf{z}_{k+1} \tag{4}$$

The estimation error mean is denoted by $\zeta_k = \mathbb{E}\left[\hat{\mathbf{x}}_{k|k} - \mathbf{x}_k\right]$. The filtering error dynamics in the interval $k_s \leq k < k_o'$ is then obtained.

$$\zeta_{k+1} = (\mathbf{I} - \mathbf{K}_{k+1}\mathbf{H})\,\boldsymbol{\Phi}^{\mathrm{CV}}\zeta_k + \mathbf{u}_k \tag{5}$$
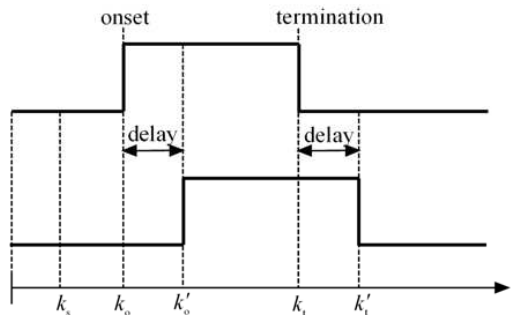
where,

$$\mathbf{u}_k = \begin{cases} 0, & k_s \leq k < k_o \\ (\mathbf{I} - \mathbf{K}_{k+1}\mathbf{H})\left(\boldsymbol{\Phi}^{\mathrm{CV}} - \boldsymbol{\Phi}^{\mathrm{CT}}\right)\bar{\mathbf{x}}_k, & k_o \leq k < k_o' \end{cases} \tag{6}$$

$\bar{\mathbf{x}}_k = \mathbb{E}\left[\mathbf{x}_k\right]$ in (6).

To guarantee the convergence of filtering, all eigenvalues λ_i, $i = 1, 2, \ldots, n$ of the matrix $(\mathbf{I} - \mathbf{K}_{k+1}\mathbf{H})\boldsymbol{\Phi}^{\mathrm{CV}}$ must be within the unit circle, i.e., the spectral radius is less than 1.

$$\rho = \max\left\{|\lambda_1|, |\lambda_2|, \ldots, |\lambda_n|\right\} < 1 \tag{7}$$

Figure 1. Motion mode switch and maneuver detection.

Since the filter is convergent and stable at the time k_s, it is reasonable to use steady-state gain $\mathbf{K}^{\mathrm{CV}}$ to approximate time-variant $\mathbf{K}_k$. The estimation error mean ζ_{k+1} can be expressed in terms of ζ_{k_s}.

$$\zeta_{k+1} = \left[\left(\mathbf{I} - \mathbf{K}^{\mathrm{CV}}\mathbf{H}\right)\boldsymbol{\Phi}^{\mathrm{CV}}\right]^{k+1-k_s}\zeta_{k_s} + \sum_{l=k_o}^{k}\left[\left(\mathbf{I} - \mathbf{K}^{\mathrm{CV}}\mathbf{H}\right)\boldsymbol{\Phi}^{\mathrm{CV}}\right]^{k-l}\mathbf{u}_l \tag{8}$$
$$(k_o \le k < k'_o)$$

The error dynamics with respect to detection delay is obtained in (8). To derive an upper bound for detection delay with certain filtering errors, we first introduce two lemmas. All norms are 2-norms unless specified otherwise in the sequel.

Lemma 1 Given an nth-order square matrix $\mathbf{A}$ with all distinct eigenvalues,

$$\left\|\mathbf{A}^l\right\| \le \kappa\left(\mathbf{A}\right)\rho^l\left(\mathbf{A}\right) \tag{9}$$

where, $\rho\left(\mathbf{A}\right)$ is the spectral radius of the matrix $\mathbf{A}$, and $\kappa\left(\mathbf{A}\right) = \|\mathbf{P}\| \cdot \|\mathbf{P}^{-1}\|$, the condition number of $\mathbf{A}$ under the inverse, where $\mathbf{P}^{-1}\mathbf{A}\mathbf{P} = \mathbf{J}_\mathbf{A}$, the Jordan canonical form.

Lemma 2 If the functions $f_1(k) = c_1 a^{k+1+s}$ and $f_2(k) = c_2 \sum_{i=0}^{k} a^i$ satisfy $c_1 a^s < \lim_{k\to\infty} f_2(k) = \frac{c_2}{1-a}$, where $0 \le a < 1$, $s \ge 1$, $c_1 > 0$, and $c_2 > 0$, the maximum of the function $f(k) = f_1(k) + f_2(k)$ is $\max_{k=\{1,2,\dots,j\}} f(k) = f(j)$.

The proof of lemmas 1 and 2 are omitted here, and the readers are referred to [13, 14].

For simplicity, let $\kappa = \kappa\left[\left(\mathbf{I} - \mathbf{K}^{\mathrm{CV}}\mathbf{H}\right)\boldsymbol{\Phi}^{\mathrm{CV}}\right]$ and $\rho = \rho\left[\left(\mathbf{I} - \mathbf{K}^{\mathrm{CV}}\mathbf{H}\right)\boldsymbol{\Phi}^{\mathrm{CV}}\right]$. According to Lemma 1, the following inequality is derived from (8).

$$\|\zeta_{k+1}\| \le \kappa\rho^{k+1-k_s}\|\zeta_{k_s}\| + \kappa U\frac{1-\rho^{k-k_o+1}}{1-\rho} \triangleq \mathrm{g}\left(k\right) \quad \left(k_o \le k < k'_o\right) \tag{10}$$

where, $U = \max\|\mathbf{u}_k\|$, $(k_o \le k < k'_o)$.

Since $\rho < 1$, $\mathrm{g}\left(k\right)$ and filtering errors are monotonically decreasing for $k < k_o$. For the time interval $k_o \le k < k'_o$. It is assumed that $\|\zeta_{k_s}\|$ satisfies the following inequality after $k_o - k_s$ iteration steps.

$$\|\zeta_{k_s}\|\rho^{k_o-k_s} < \frac{U}{1-\rho} \tag{11}$$

Let $c_1 = \|\zeta_{k_s}\|$; $c_2 = U$; $s = k_o - k_s$. From Lemma 2, we know that $\mathrm{g}\left(k\right)$ is monotonically increasing for $k_o \le k < k'_o$, that is, the filtering is divergent.

In order to perform tracking continuously and not to miss the target, it is necessary to restrict the filtering errors less than the maximum allowed one E_0.

$$g\left(k_o'\right) = \kappa\rho^{k_o'+1-k_s} \left\|\zeta_{k_s}\right\| + \kappa U \frac{1 - \rho^{k_o'-k_o+1}}{1 - \rho} \le E_0 \qquad (12)$$

From (12), we get the upper bound for maneuver detection delay $\Delta = k_o' - k_o$.

$$\Delta = k_o' - k_o \le \frac{1}{\ln\rho} \ln\left|1 - \frac{E_0\left(1 - \rho\right)}{\kappa U}\right| - 1 \qquad (13)$$

We actually obtain the upper bound for maneuver onset detection delay. Similar analysis can be performed on the time interval $k_o' \le k < k_t'$ for maneuver termination detection. The results are important for maneuver detector design. In many applications, e.g., aerial defense, homing guidance, where targets maintain high speed and maneuverability, it is thus fairly demanding for maneuver detector. However, traditional detectors are incapable of low detection delay. We next introduce a feature aided one. It is noted that Kalman filter is an approximately optimal estimator for the base-state in a linear Gaussian hybrid system. So the deduction of the upper bound for the detection delay is using the standard Kalman filter.

3. FEATURE AIDED MANEUVER DETECTOR

A brief introduction of feature aided maneuver detector is given in this section. Nonmaneuvering and maneuvering motion modes are identified using the differences in the resolution of HRDP. The readers are referred to [11] for more details.

3.1. Detection Principle

Since aerial targets must obey aerodynamics, the motion mode switch will lead to the changes of pose angle. We next derive the pose angular rates under different motion modes. For simplicity, we consider two-dimensional planar encounter geometry as shown in Fig. 2.

The polar coordinates of target position in the inertial frame are (r, φ), and the coordinates of radar position in the structural frame are (r, ϕ). The rotational angle of the structural frame with respect to the inertial frame is ψ, which is known as Euler angle. Since radar signatures are concerned, we turn our attention to target pose angle ϕ. It varies with target motion. However, the angular rates are distinct under different motion modes. In Fig. 2, the pose angle is

$$\phi = \pi + \varphi - \psi \qquad (14)$$
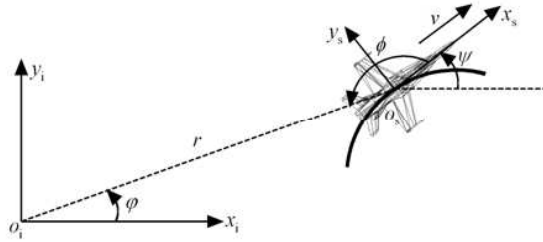
Figure 2. Two-dimensional planar encounter geometry.

Assumed that target speed is v, and the tangential and normal accelerations are a_t and a_n, respectively. By taking derivative of (14) and applying the rigid body kinematical equations, we obtained

$$\dot{\phi} = \frac{v\sin\phi + a_t t\sin\phi + a_n t\cos(\varphi+\psi)}{r_0 - 2vt\cos\phi - a_t t^2\cos\phi + a_n t^2\sin(\varphi+\psi)} - \frac{a_n}{v} \qquad (15)$$

where, r_0 is the target initial range.

We next discuss the pose angular rates under different motion modes.

3.1.1. Nonmaneuvering Motion Mode

If target is nonmaneuvering, its velocity is constant and accelerations are zero, i.e., $a_t = a_n = 0$. It is known as CV motion mode [12]. The pose angular rate is obtained from (15)

$$\dot{\phi}_{\rm CV} = \frac{v\sin\phi}{r_0 - 2vt\cos\phi} \qquad (16)$$

Target range is usually far, and the pose angular rate is a very small value.

3.1.2. Maneuvering Motion Mode

Since (15) is a little complicated, we consider the following two special cases.

(a) If $a_t = 0$ and $a_n = $ constant, target has a constant speed and a constant turn rate, which is referred to as CT motion mode [12]. (15) is then simplified as

$$\dot{\phi}_{\rm CT} = \frac{v\sin\phi + a_n t\cos(\varphi+\psi)}{r_0 - 2vt\cos\phi + a_n t^2\sin(\varphi+\psi)} - \frac{a_n}{v} \qquad (17)$$

Comparing with $\dot{\phi}_{\rm CV}$, we find an additional item a_n/v in $\dot{\phi}_{\rm CT}$. It is the item that $\left|\dot{\phi}_{\rm CT}\right| \gg \left|\dot{\phi}_{\rm CV}\right|$ holds. The pose angular rate under CT motion mode is much greater than that under CV motion mode.

(b) If $a_n = 0$ and $a_t = $ constant, target is under constant acceleration (CA) motion mode [12]. Then we have

$$\dot{\phi}_{\mathrm{CA}} = \frac{v \sin \phi + a_t t \sin \phi}{r_0 - 2vt \cos \phi - a_t t^2 \cos \phi} \tag{18}$$

The pose angular rate $\dot{\phi}_{\mathrm{CA}}$ is approximately equal to $\dot{\phi}_{\mathrm{CV}}$, as tangential acceleration is generally small in magnitude and of short duration. Therefore, the pose angular rate $\dot{\phi}_{\mathrm{CA}}$ is also a small value.

From above analysis, target pose angular rates are distinct under different motion modes. Specifically, it is much greater under normal accelerated motion mode (e.g., CT motion mode) than that under nonmaneuvering and tangential accelerated motion modes (e.g., CV and CA motion modes). Fortunately, normal accelerated motion mode, especially CT motion mode, is frequently discussed by tracking community not only because it is the motion mode that targets, especially military targets, prefer to performing during a combat but also because it has a significant impact on target tracking performance. It is pointed out in [15] that accelerations in the velocity direction (drag and thrust) are generally smaller in magnitude and of shorter duration than the lift (normal) accelerations over most realistic flight regimes.

3.2. Maneuver Detector

As shown in Fig. 2, if radar transmits high pulse repetition frequency (HPRF) waveform, the baseband signal after motion compensation is [16]

$$G(n) = \int \sigma(\mathbf{x}) \exp\left(-\mathrm{j}\frac{4\pi f_0}{c} \mathbf{r}_n \cdot \mathbf{x}\right) \mathrm{d}\mathbf{x} \tag{19}$$

where $\sigma(\mathbf{x})$ is the target reflectivity distribution and $\mathbf{r}_n$ the unit vector parallel to $o_i o_s$ at the time when the nth pulse is transmitted. The integration is carried out over the volume of target. (19) represents the samples of the Fourier transform of the reflectivity collected along an arc of the circumference [16].

By taking inverse discrete Fourier transform (IDFT) of the sequence $G(n)$, a discrete one-dimensional profile of the target reflectivity along the cross-range, i.e., HRDP, is obtained. The resolution of HRDP Δl turns out to be inversely proportional to the variation of the pose angle $\Delta\phi$, i.e.,

$$\Delta l = \frac{\lambda}{2 \sin \Delta\phi} \tag{20}$$

where λ is the wavelength.

From the resolution formula (20), a minimum variation of pose angle is required to obtain target HRDP. Consequently, the coherent processing interval (CPI) can be appropriately determined, so that the variation of pose angle is less than what is the required when the target performs nonmaneuvering motion and that the variation of pose angle meets the profiling requirements when the target performs maneuvering motion. Therefore, it is unable to distinguish scatterers from target HRDP, and the target behaves as a point target under nonmaneuvering situation. On the other hand, under maneuvering situation it is able to distinguish multiple scatterers from target HRDP, and the target behaves as an extended target. This is the principle of the maneuver detection using HRDP.

From (19), target HRDP is sensitive to pose angle, and is nonstationary during target motion. Using the classical approach to design a detector is too difficult. The maneuver detection problem is reformulated as an adaptive pattern classification problem in this paper [17]. Different classes such as maneuvering and nonmaneuvering motion mode are distinguished. A classifier based on back propagation (BP) neural network (NN) is developed. The developed NN is made up of three layers. The outputs are linearly combined to produce the final output, where the final decision is made. The block diagram of the detector and the detailed architecture of the NN are shown in Fig. 3. A comprehensive performance evaluation is presented in [11], and low detection delay and high detection probability are gained.

4. SWITCHING MODEL-SET FILTERING ALGORITHM

4.1. State Space Model

The motion model is given by (1). However, the magnitude and direction of target turn rate is hardly to know in practice. We use a model set containing multiple models to describe target maneuvering
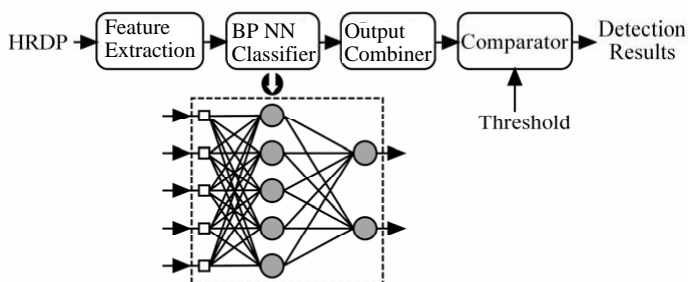
**Figure 3.** Block diagram of detector and detailed architecture of NN.

motion mode. For model-set design, it is still a challenging topic. At present, only Li et al. [18] have discussed it and proposed three classes of methods. For brevity, we choose two models, i.e., left turn and right turn models. The model set is $\mathbb{M}_1 = \{+\omega, -\omega\}$ under maneuvering motion mode. The turn rate magnitude ω has to be determined according to the specific application [18]. Obviously, the model-set for nonmaneuvering motion mode is $\mathbb{M}_0 = \{0\}$.

(2) is the measurement model. Actually, target positions are obtained in sensor coordinates, and it is spherical in three-dimensional space with range, azimuth (or bearing), and elevation. For simplicity, we describe measurement equation in Cartesian coordinates, and assume that target positions are measurable. Fortunately, many approaches have proposed to resolve the nonlinearity, for instance, converted measurements method is a commonly used one [19].

4.2. Filtering Algorithm

4.2.1. Principle

The diagram of feature aided switch model set filtering algorithm is shown in Fig. 4. Once echo signals are received, HRDPs and measurements of the target are extracted and sent to the detector and filter, respectively. The unique model-set for filtering is switched from $\mathbb{M}_0$ to $\mathbb{M}_1$ and vice versa according to the feature aided maneuver detection results, hence the name feature aided switching model-set
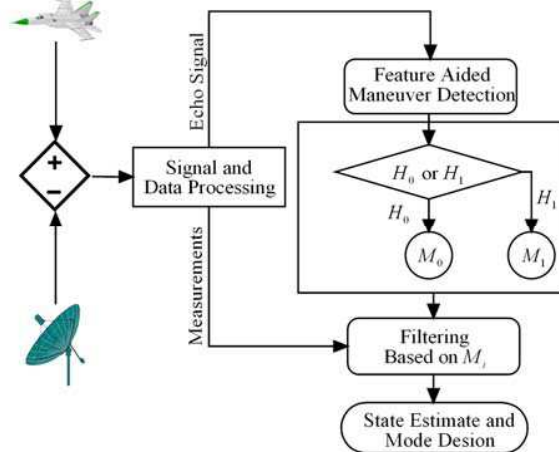
Figure 4. Diagram of filtering algorithm.

filtering. Since a time-varying model-set is used for filtering, the proposed algorithm can be regarded as a variable-structure multiple model (VSMM) method. Thus, the VSMM algorithm in the sequel represents our proposed switching model-set filtering algorithm.

4.2.2. Model-set Conditioned Filtering

Since the model set $\mathbb{M}_0$ contains only CV model. It is optimal to use standard Kalman filter. It is omitted here. We present model set $\mathbb{M}_1$ conditioned filtering algorithm. As stated that $\mathbb{M}_1 = \{+\omega, -\omega\}$, containing left and right turn models. Therefore, MM method will be employed under maneuvering motion mode. It is optimal to use autonomous MM (AMM) algorithm [5].

Step 1. Model-conditioned filtering (for $i = 1, 2$):

Predicted state: $\hat{\mathbf{x}}_{k+1|k}^{(i)} = \boldsymbol{\Phi}_{\mathrm{CT}}^{(i)} \hat{\mathbf{x}}_{k|k}^{(i)}$

Predicted covariance: $\mathbf{P}_{k+1|k}^{(i)} = \boldsymbol{\Phi}_{\mathrm{CT}}^{(i)} \mathbf{P}_{k|k}^{(i)} \left[\boldsymbol{\Phi}_{\mathrm{CT}}^{(i)} \right]^T + \mathbf{Q}_{\mathrm{CT}}^{(i)}$

Measurement residual: $\tilde{\mathbf{z}}_{k+1}^{(i)} = \mathbf{z}_{k+1}^{(i)} - \mathbf{H}\hat{\mathbf{x}}_{k+1|k}^{(i)}$

Residual covariance: $\mathbf{S}_{k+1}^{(i)} = \mathbf{H}\mathbf{P}_{k+1|k}^{(i)} \mathbf{H}^T + \mathbf{R}$

Filter gain: $\mathbf{K}_{k+1}^{(i)} = \mathbf{P}_{k+1|k}^{(i)} \mathbf{H}^T \left[\mathbf{S}_{k+1}^{(i)} \right]^{-1}$

Update state: $\hat{\mathbf{x}}_{k+1|k+1}^{(i)} = \hat{\mathbf{x}}_{k+1|k}^{(i)} + \mathbf{K}_{k+1}^{(i)} \tilde{\mathbf{z}}_{k+1}^{(i)}$

Update covariance: $\mathbf{P}_{k+1|k+1}^{(i)} = \mathbf{P}_{k+1|k}^{(i)} - \mathbf{K}_{k+1}^{(i)} \mathbf{S}_{k+1}^{(i)} \left[\mathbf{K}_{k+1}^{(i)} \right]^T$

Step 2. Model probability update (for $i = 1, 2$):

Model likelihood:

$$L_k^{(i)} = \mathcal{N}\left(\tilde{\mathbf{z}}_{k+1}^{(i)}; \mathbf{0}, \mathbf{S}_{k+1}^{(i)} \right) = \frac{1}{\left| 2\pi \mathbf{S}_{k+1}^{(i)} \right|^{1/2}} \exp\left[-\frac{\left[\tilde{\mathbf{z}}_{k+1}^{(i)} \right]^T \left[\mathbf{S}_{k+1}^{(i)} \right]^{-1} \tilde{\mathbf{z}}_{k+1}^{(i)}}{2} \right]$$

Mode probability: $\mu_{k+1}^{(i)} = \frac{\mu_k^{(i)} L_{k+1}^{(i)}}{\sum_j \mu_k^{(j)} L_{k+1}^{(j)}}$

Step 3. Estimate fusion:

Overall estimate: $\hat{\mathbf{x}}_{k+1|k+1} = \sum_i \hat{\mathbf{x}}_{k+1|k+1}^{(i)} \mu_{k+1}^{(i)}$

Overall covariance:

$$\mathbf{P}_{k+1|k+1} = \sum_i \left[\mathbf{P}_{k+1|k+1}^{(i)} + \left(\hat{\mathbf{x}}_{k+1|k+1} - \hat{\mathbf{x}}_{k+1|k+1}^{(i)} \right) \left(\hat{\mathbf{x}}_{k+1|k+1} - \hat{\mathbf{x}}_{k+1|k+1}^{(i)} \right)^T \right] \mu_{k+1}^{(i)}$$

4.2.3. Filter Initialization

The tracking filter can be initialized using two-point method. Once target maneuver is detected, the filters can be initialized as follows.

$$\hat{\mathbf{x}}_{k+1|k+1}^{(i)} = \hat{\mathbf{x}}_{k+1|k+1}, \mathbf{P}_{k+1|k+1}^{(i)} = \mathbf{P}_{k+1|k+1}, \mu_{k+1}^{(i)} = 1/|M_1|$$
$$(i = \mathrm{CV}, \mathrm{CT}) \quad (21)$$

where, $|\cdot|$ denotes the cardinality of a set.

5. SIMULATION EXPERIMENTS

5.1. Simulation Scenario

The target fighter F18 initially locates at the height of 6000 feet. It performs straight and level motion with a nearly constant velocity 0.8 mach in the first second, and then performs a 6 g (g is the gravitational acceleration) constant turn maneuver for another 3 seconds. The effects of different distances and attitudes between radar and target have to be minimized in the experiment. Therefore, the radar positions are chosen at random in the horizontal plane. The horizontal distances uniformly distribute between 20 km and 50 km, while the azimuths uniformly distribute between 0° and 360°. One thousand Monte Carlo experiments are run. In addition, a simulation platform is developed
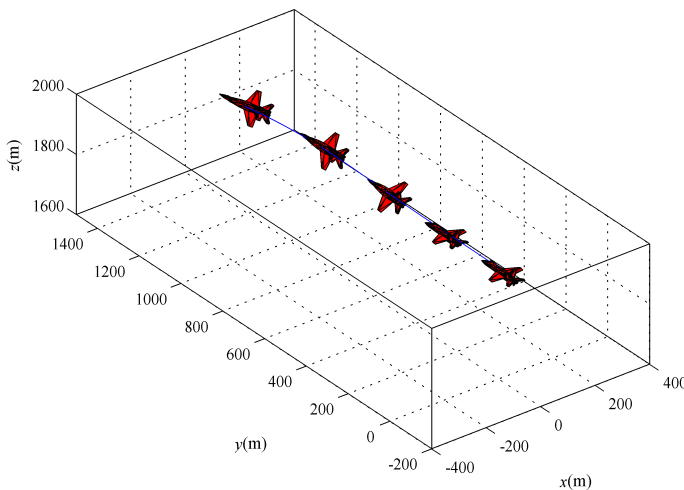
Figure 5. Simulated target trajectory.

for echo signal generation [11]. Fig. 5 shows the simulated target trajectory in the experiment.

5.2. Simulation Results

5.2.1. Detection Delay and Error Dynamics

In the above scenario, we perform a numerical simulation on detection delay and error dynamics. Fig. 6 shows the results of error dynamics with different detection delays. The filtering errors decrease continuously before target maneuvers. However, once it begins to maneuver, the position and velocity errors increase due to mode-model mismatch. The greater the detection delay, the larger the filtering errors. When maneuver is correctly detected, the filtering errors are convergent again.

Figure 7 shows detection delay bounds with respect to different normal accelerations and maximum allowed errors. Given a normal acceleration and turn rate, detection delay upper bounds turn out to be greater with larger error bounds, that is, it allows a longer time mode-model mismatch. On the other hand, given the maximum allowed error, detection delay upper bounds turn out to be smaller with larger normal accelerations and turn rates, that is, the higher the target maneuverability, the smaller upper bound for the detection delay. For instance, if the maximum allowed error $E_0 = 100$ and target normal acceleration is $6\,g$ in our experiment, the upper bound for detection delay is about $0.5\,s$. In fact, this is fairly demanding for maneuver detector. From [11], we find out that the detection probability of the feature aided maneuver detector becomes about 90% at the time of
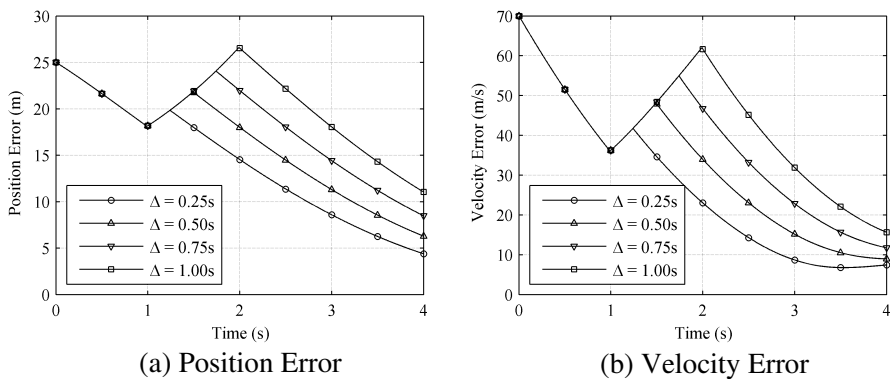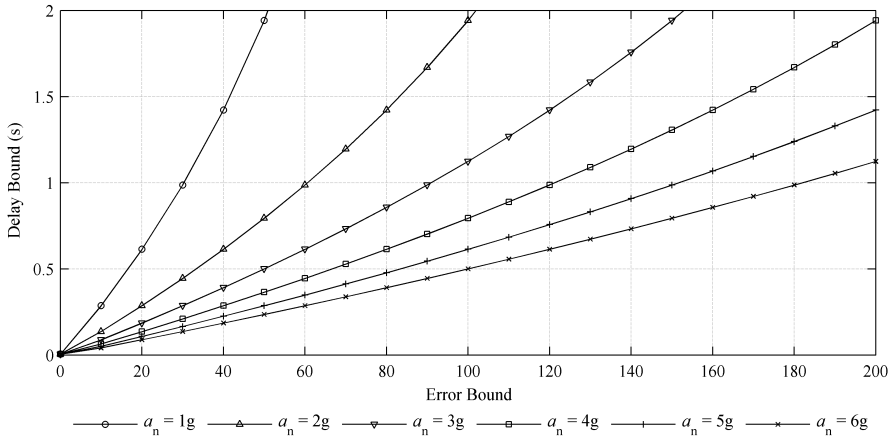

(a) Position Error   (b) Velocity Error

Figure 6. Error dynamics with different detection delays.

Figure 7. Detection delay bounds with respect to different normal accelerations and maximum allowed errors.

Table 1. Parameters of filtering algorithms.

Parameters		Value
Power spectral density of process noise	CV model m_0	1
	CT model m_1	1
	CT model m_2	1
Standard deviation of measurement noise	x	50 m
	y	50 m
Model transition probability matrix	$\begin{bmatrix} 0.950 & 0.025 & 0.025 \\ 0.025 & 0.950 & 0.025 \\ 0.025 & 0.025 & 0.950 \end{bmatrix}$	

0.5 s delay, while that of the detector using range rate measurements remains at a considerably low level [20].

5.2.2. Filtering Results

Since the proposed switching model-set filtering algorithm can be regarded as a VSMM method, we also do tracking using the first two generation MM methods, i.e., AMM and cooperating MM (CMM), for performance evaluation. We choose the most popular interacting MM (IMM) algorithm from a lot of CMM algorithms. Table 1 lists the parameters of the tracking filters.
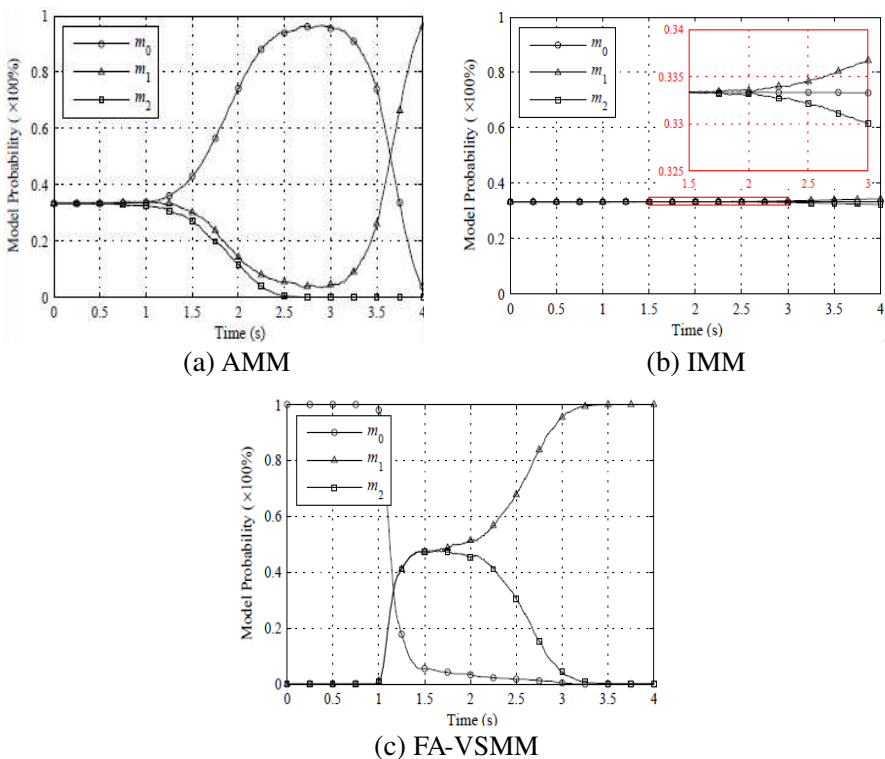
(a) AMM

(b) IMM

(c) FA-VSMM

Figure 8. Model probability histories.
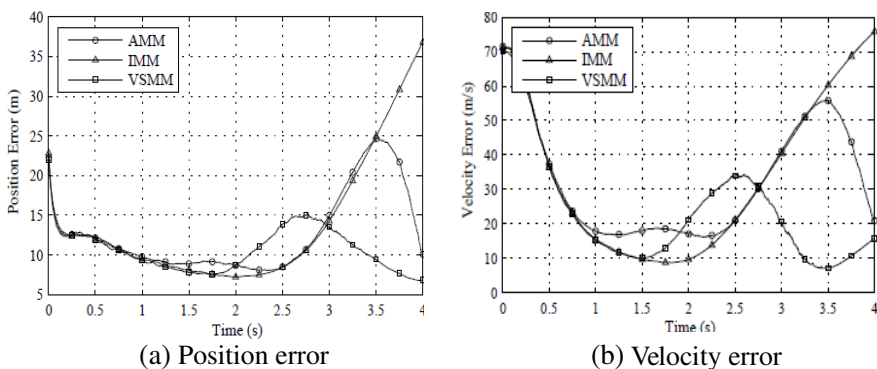

(a) Position error

(b) Velocity error

Figure 9. Filtering errors of the three algorithms.

Figure 8 shows the model probability histories of the three MM algorithms. For $0 \leq t < 1\,\mathrm{s}$, target is nonmaneuvering, and CV model matching with target motion mode is employed in VSMM algorithm. The designed model-set constituted of three models is employed in AMM and IMM algorithms. Their probabilities keep nearly the same, that is, the correct model is not identified. This may be due to the two CT models with the same turn rate and opposite turn directions, and the filtering performance is close to that of CV model. We also see that the filtering errors of the three MM methods show slight differences in Fig. 9. For $t > 1\,\mathrm{s}$, target is maneuvering, the probability of the true model reaches the greatest after a certain delay time, that is, the motion mode can be correctly identified by all three MM algorithms. VSMM algorithm achieves that earliest, and the probability of model m_1 reaches the greatest at $t = 1.61\,\mathrm{s}$. AMM algorithm gets that latest, and at $t = 3.66\,\mathrm{s}$ the correct model is identified.

Comparing with Figs. 8(a) and 8(c), the probability histories of the three models in Fig. 8(b) change with time very slowly as IMM algorithm performs interacting step [5].

Figure 9 shows the filtering errors of the three MM algorithms. Overall VSMM algorithm performs best out of the three, the filtering errors remain small. They increase slightly as the probability is converging, and decrease to a considerably low level subsequently. The filtering errors of AMM and IMM algorithms accumulate and increase with time. For AMM algorithm, once the correct model is identified, the filtering errors decrease significantly. However, the filtering errors of IMM algorithm remain increasing, since the probability of the correct model converge too slowly.

6. CONCLUSIONS

A feature aided switching model-set approach for MTT is proposed in this paper. We first present error dynamics with respect to detection delay, and access the upper bound for detection delay with given maximum allowed errors. The results are useful for maneuver detector design, and also show that low detection delay is necessary for small filtering errors in many applications. Therefore, a feature aided maneuver detector is introduced to enhance the detection performance. The filtering model-set is chosen according to the detection results. The detailed filtering steps of switching model-set approach are presented, including computation formulae. Simulation results show that the proposed algorithm outperforms the other two generation MM algorithms, i.e., AMM and IMM.

REFERENCES

1. Wang, X. F., J. F. Chen, Z. G. Shi, and K. S. Chen, "Fuzzy-control-based particle filter for maneuvering target tracking," *Progress In Electromagnetics Research*, Vol. 118, 1–15, 2011.

2. Hong, S., L. Wang, Z.-G. Shi, and K. S. Chen, "Simplified particle PHD filter for multiple-target tracking: Algorithm and architecture," *Progress In Electromagnetics Research*, Vol. 120, 481–498, 2011.

3. Li, X. R. and V. P. Jilkov, "A survey of maneuvering target tracking — Part IV: Decision-based methods," *Proceedings of the SPIE Conference on Signal and Data Processing of Small Targets*, Vol. 4728, 511–534, Orlando, FL, USA, April 2002.

4. Ru, J., V. P. Jilkov, X. R. Li, and A. Bashi, "Detection of target maneuver onset," *IEEE Transactions on Aerospace and Electronic Systems*, Vol. 45, No. 2, 536–554, April 2009.

5. Li, X. R. and V. P. Jilkov, "Survey of maneuvering target tracking. Part V: Multiple-model methods," *IEEE Transactions on Aerospace and Electronic Systems*, Vol. 41, No. 4, 1255–1321, October 2005.

6. Bizup, D. F. and D. E. Brown, "Maneuver detection using the radar range rate measurement," *IEEE Transactions on Aerospace and Electronic Systems*, Vol. 40, No. 1, 330–336, January 2004.

7. Shetty, S. and A. T. Alouani, "A multisensor tracking system with an image-based maneuver detector," *IEEE Transactions on Aerospace and Electronic Systems*, Vol. 32, No. 1, 167–181, January 1996.

8. Hughes, E. J. and M. Leyland, "Target maneuver detection using radar glint," *Electronics Letters*, Vol. 34, No. 17, 1695–1696, August 1998.

9. Fan, H., "Technology on maneuvering target motion mode identification in active homing guidance," Ph.D. dissertation, National University of Defense Technology, Changsha, December 2008.

10. Yang, C. and E. Blasch, "Estimating target range-doppler image slope for maneuver indication," *Proceedings of 2008 SPIE Conference on Signal Processing, Sensor Fusion, and Target Recognition XVII*, Vol. 6968, Orlando, FL, USA, March 2008.

11. Zhu, Y., H. Fan, J. Fan, Z. Lu, and Q. Fu, "Target turing maneuver detection using high resolution doppler profile," *IEEE Transactions on Aerospace and Electronic Systems*, Vol. 48, No. 1, 762–779, 2012.

12. Li, X. R. and V. P. Jilkov, "Survey of maneuvering target tracking.

Part I: Dynamic models," *IEEE Transactions on Aerospace and Electronic Systems*, Vol. 39, No. 4, 1333–1363, October 2003.

13. Hwang, I., H. Balakrishnan, and C. Tomlin, "Observability criteria and estimator design for stochastic linear hybrid systems," *Proceedings of IEE European Control Conference*, 2003.

14. Fan, H., Y. Zhu, and Q. Fu, "Impact of mode decision delay on estimation error for maneuvering target interception," *IEEE Transactions on Aerospace and Electronic Systems*, Vol. 47, No. 1, 702–711, January 2011.

15. Kendrick, J. D., P. S. Maybeck, and J. G. Reid, "Estimation of aircraft target motion using orientation measurements," *IEEE Transactions on Aerospace and Electronic Systems*, Vol. 17, No. 2, 254–260, March 1981.

16. Berizzi, F. and G. Corsini, "Autofocusing of inverse synthetic aperture radar images using contrast optimization," *IEEE Transactions on Aerospace and Electronic Systems*, Vol. 32, No. 3, 1185–1191, July 1996.

17. Haykin, S. and D. J. Thomson, "Signal detection in a nonstationary environment reformulated as an adaptive pattern classification problem," *Proceedings of the IEEE*, Vol. 86, No. 11, 2325–2344, November 1998.

18. Li, X. R., Z. Zhao, and X.-B. Li, "General model-set design methods for multiple-model approach," *IEEE Transactions on Automatic Control*, Vol. 50, No. 9, 1260–1276, September 2005.

19. Li, X. R. and V. P. Jilkov, "A survey of maneuvering target tracking — Part III: Measurement models," *Proceedings of SPIE Conference on Signal and Data Processing of Small Targets*, Vol. 4473, 423–446, San Diego, CA, USA, July–August 2001.

20. Ru, J., H. Chen, X. R. Li, and G. Chen, "A range rate based detection technique for tracking a maneuvering target," *Proceedings of SPIE Conference on Signal and Data Processing of Small Targets*, Vol. 5913, 59 131Q-1–59 131Q-13, San Diego, CA, USA, August 2005.